TENSOR COMPLETION VIA GLOBAL LOW-TUBAL-RANKNESS AND NONLOCAL SELF-SIMILARITY

Tian Lu, Xi-Le Zhao*, Yu-Bang Zheng, Meng Ding, Xiao-Tong Li

School of Mathematical Sciences/Reserarch Center for Image and Vision Computing,
University of Electronic Science and Technology of China, Chengdu, P. R. China

ABSTRACT

The recent popular tensor nuclear norm (TNN), a convex surrogate of tensor tubal rank, obtains promising results in tensor completion. Although the TNN-based model has shown its prominent capability of characterizing the global structure of tensors, it lacks the capability for preserving the abundant details of the target tensor. By integrating the global low-tubal-rankness and nonlocal self-similarity, we propose a novel tensor completion model, which recovers the global structural information by TNN regularizer while compensating for the details by plugging in a denoiser to express the nonlocal self-similarity prior. We design an alternating directional method of multipliers (ADMM)-based algorithm to solve the proposed model. Extensive experimental results on color images and fluorescence microscope images demonstrate the superiority of the proposed method over the compared ones.

Index Terms— Nonlocal self-similarity, tensor nuclear norm, tensor completion, plug-and-play, alternating direction method of multipliers.

1. INTRODUCTION

As the higher dimensional extension of matrices, tensors provide an effective form to express the structural properties of higher-order data. Due to inevitable degradation in the acquisition process, the tensor completion problem has gained its increasing importance. Since the tensor rank is capable of efficiently catching the global information of the target tensor, many tensor completion methods are devoted to minimizing the tensor rank. Mathematically, the low-rank tensor completion (LRTC) model can be formulated as:

$$\arg \min_{\mathcal{X}} \text{rank}(\mathcal{X}), \quad \text{s.t.} \quad \mathcal{P}_\Omega(\mathcal{X}) = \mathcal{P}_\Omega(\mathcal{M}),$$

where $\mathcal{X}$ is the underlying tensor, $\mathcal{M}$ is the observed tensor, Ω is the index set of the observed entries, and $\mathcal{P}_\Omega(\cdot)$ is the projection function, which keeps the entries of $\mathcal{X}$ in Ω while making others be zeros.

However, there is no consensus on the most appropriate

---

definition of tensor rank. And directly minimizing the tensor rank is NP-hard [1]. Therefore, the common practice is to design convex or non-convex [2, 3] surrogate optimization alternatives based on different definitions [4].

Recently, the tensor tubal rank defined based on tensor singular value decomposition (t-SVD) has shown its effectiveness to exploit the inherent low-rank structure of a tensor [5–8]. Inspired by the success of matrix nuclear norm, the tensor nuclear norm (TNN) is used as a convex surrogate for the tubal rank [9], and the corresponding LRTC model can be rewritten as:

$$\arg \min_{\mathcal{X}} ||\mathcal{X}||_*, \quad \text{s.t.} \quad \mathcal{P}_\Omega(\mathcal{X}) = \mathcal{P}_\Omega(\mathcal{M}), \quad (1)$$

where $||\mathcal{X}||_*$ is the TNN of tensor $\mathcal{X}$ (see details in Section 2).

Although the TNN-based model shows its effectiveness to preserve the intrinsic structure of the tensor [10, 11], it only considers the global correlation, which could cause the recovered tensor to lose abundant details. In fact, not limited to the global correlation, the real-world data have the property of nonlocal self-similarity. Recently, the nonlocal self-similarity [12], which exploits the spatial redundancy of nonlocal similar patches, has emerged as one of the most successful regularizations for natural images.

The above analyses motivate us to take nonlocal self-similarity into consideration. In this paper, we introduce an implicit regular term to exploit the nonlocal self-similarity. The proposed model contains two terms, one for the low-rankness and another for the nonlocal self-similarity, i.e.,

$$\arg \min_{\mathcal{X}} ||\mathcal{X}||_* + \lambda \Phi(\mathcal{X}), \quad \text{s.t.} \quad \mathcal{P}_\Omega(\mathcal{X}) = \mathcal{P}_\Omega(\mathcal{M}).$$

Instead of tailoring nonlocal regularizers, we tackle with the implicit regularizer $\Phi(\mathcal{X})$ by plugging in an off-the-shell denoiser to express the nonlocal self-similarity prior and design a plug-and-play (PnP) [13] alternating direction method of multipliers (ADMM) framework to solve the model.

The rest of this paper is organized as follows. Section 2 gives some notations and preliminaries. Section 3 introduces the proposed model and algorithm. Section 4 reports the results of the proposed method by numerical experiments. Section 5 concludes this paper.

2. NOTATIONS AND PRELIMINARIES

In this section, we give a brief overview of t-SVD [9]. For a third-order tensor $\mathcal{A} \in \mathbb{R}^{n_1 \times n_2 \times n_3}$, we use $\mathcal{A}(k,:,:)$, $\mathcal{A}(:,k,:)$, and $\mathcal{A}(:,:,k)$ to denote the k_{th} horizontal, lateral, and frontal slice, which corresponds with the notations in Matlab. Especially, the i_{th} frontal slice is also be represented by $\mathcal{A}^{(i)}$. We use $\bar{\mathcal{A}}$ to denote the tensor generated by performing Discrete Fourier Transformation (DFT) along each tube of $\mathcal{A}$, i.e., $\bar{\mathcal{A}} = \texttt{fft}(\mathcal{A}, [], 3)$.

Definition 1 (t-product [9]) The t-product $\mathcal{C} = \mathcal{A} * \mathcal{B}$ of $\mathcal{A} \in \mathbb{R}^{n_1 \times n_2 \times n_3}$ and $\mathcal{B} \in \mathbb{R}^{n_2 \times n_4 \times n_3}$ is defined as

$$\mathcal{C}(i,j,:) = \sum_{k=1}^{n_2} \mathcal{A}(i,k,:) * \mathcal{B}(k,j,:),$$

where the operation $*$ is circular convolution.

Definition 2 (Conjugate transpose [9]) The conjugate transpose of a tensor $\mathcal{A} \in \mathbb{R}^{n_1 \times n_2 \times n_3}$ is denoted as $\mathcal{A}^*$, which is obtained by conjugate transposing each of the frontal slice and then reversing the order of transposed frontal slices 2 through n_3.

Definition 3 (Identity tensor [9]) The identity tensor $\mathcal{I} \in \mathbb{R}^{n_1 \times n_2 \times n_3}$ is the tensor whose first frontal slice is the identity matrix, and other frontal slices are all zeros.

Definition 4 (Orthogonal Tensor [9]) A third-order tensor $\mathcal{Q} \in \mathbb{R}^{n_1 \times n_2 \times n_3}$ is orthogonal if

$$\mathcal{Q} * \mathcal{Q}^* = \mathcal{Q}^* * \mathcal{Q} = \mathcal{I}.$$

Definition 5 (f-diagonal tensor [9]) A tensor is called f-diagonal if each of its frontal slice is a diagonal matrix.

Definition 6 (t-SVD [9]) The tensor $\mathcal{A} \in \mathbb{R}^{n_1 \times n_2 \times n_3}$ can be decomposed as

$$\mathcal{A} = \mathcal{U} * \mathcal{S} * \mathcal{V}^*,$$

where $\mathcal{U} \in \mathbb{R}^{n_1 \times n_1 \times n_3}$ and $\mathcal{V} \in \mathbb{R}^{n_2 \times n_2 \times n_3}$ are orthogonal, and $\mathcal{S} \in \mathbb{R}^{n_1 \times n_2 \times n_3}$ is a f-diagonal tensor.

Note that we can efficiently obtain the decomposition by computing a series of matrix SVDs in the Fourier domain [9].

Definition 7 (Tensor multi-rank [9]) The multi-rank of $\mathcal{A} \in \mathbb{R}^{n_1 \times n_2 \times n_3}$ is a vector $r \in \mathbb{R}^{n_3}$, whose i_{th} element is the rank of the i_{th} frontal slice of $\bar{\mathcal{A}}$.

Definition 8 (Tensor tubal rank [9]) The tubal rank of $\mathcal{A} \in \mathbb{R}^{n_1 \times n_2 \times n_3}$ is defined as the number of nonzero singular tubes of $\mathcal{S}$, where $\mathcal{S}$ is from the t-SVD of $\mathcal{A} = \mathcal{U} * \mathcal{S} * \mathcal{V}^*$.

Definition 9 (Tensor nuclear norm(TNN) [9]) The tensor nuclear norm of $\mathcal{A} \in \mathbb{R}^{n_1 \times n_2 \times n_3}$, denoted as $||\mathcal{A}||_*$, is defined as the sum of singular values of all the frontal slices of $\bar{\mathcal{A}}$, i.e.,

$$||\mathcal{A}||_* = \sum_{i=1}^{n_3} ||\bar{\mathcal{A}}^{(i)}||_*.$$

3. PROPOSED MODEL AND ALGORITHM

3.1. Proposed Model

Considering a third-order tensor $\mathcal{X} \in \mathbb{R}^{n_1 \times n_2 \times n_3}$, the proposed LRTC model can be written as follows:

$$
\begin{aligned}
\arg\min_{\mathcal{X}} \quad & ||\mathcal{X}||_* + \lambda\Phi(\mathcal{X}), \\
\text{s.t.} \quad & \mathcal{P}_\Omega(\mathcal{X}) = \mathcal{P}_\Omega(\mathcal{M}),
\end{aligned}
\tag{2}
$$

where λ is the regular parameter, $\Phi(\mathcal{X})$ is the regularization term and $\mathcal{M}$ is the observed tensor.

3.2. Proposed Algorithm

By introducing auxiliary variables $\mathcal{Y}$ and $\mathcal{Z}$, we can rewrite (2) as follows:

$$
\begin{aligned}
\arg\min_{\mathcal{X},\mathcal{Y},\mathcal{Z}} \quad & ||\mathcal{Y}||_* + \lambda\Phi(\mathcal{Z}) + \iota(\mathcal{X}), \\
\text{s.t.} \quad & \mathcal{X} - \mathcal{Z} = 0, \\
& \mathcal{X} - \mathcal{Y} = 0,
\end{aligned}
\tag{3}
$$

where $\iota(\mathcal{X})$ denotes the indicator function, i.e.,

$$
\iota(\mathcal{X}) = \begin{cases} 0, & (i,j,k) \in \Omega, \\ \infty, & \text{otherwise.} \end{cases}
\tag{4}
$$

Then the augmented Lagrangian function is:

$$
\begin{aligned}
L_{\beta_1,\beta_2}&(\mathcal{X},\mathcal{Y},\mathcal{Z},\Lambda_1,\Lambda_2) = ||\mathcal{Y}||_* + \lambda\Phi(\mathcal{Z}) + <\mathcal{X} - \mathcal{Y}, \Lambda_1> \\
&+ \frac{\beta_1}{2}||\mathcal{X} - \mathcal{Y}||_F^2 + <\mathcal{X} - \mathcal{Z}, \Lambda_2> + \frac{\beta_2}{2}||\mathcal{X} - \mathcal{Z}||_F^2 + \iota(\mathcal{X}).
\end{aligned}
\tag{5}
$$

According to the framework of ADMM, we solve (5) by the following iterative scheme:

$$
\begin{cases}
\mathcal{Y}^{k+1} = \arg\min_{\mathcal{Y}} ||\mathcal{Y}||_* + \dfrac{\beta_1}{2}||\mathcal{X}^k - \mathcal{Y} + \dfrac{\Lambda_1^k}{\beta_1}||_F^2, \\[2mm]
\mathcal{Z}^{k+1} = \arg\min_{\mathcal{Z}} \lambda\Phi(\mathcal{Z}) + \dfrac{\beta_2}{2}||\mathcal{X}^k - \mathcal{Z} + \dfrac{\Lambda_2^k}{\beta_2}||_F^2, \\[2mm]
\mathcal{X}^{k+1} = \arg\min_{\mathcal{X}} \dfrac{\beta_1}{2}||\mathcal{X}^k - \mathcal{Y} + \dfrac{\Lambda_1^k}{\beta_1}||_F^2 \\[2mm]
\qquad\quad + \dfrac{\beta_2}{2}||\mathcal{X}^k - \mathcal{Z} + \dfrac{\Lambda_2^k}{\beta_2}||_F^2 + \iota(\mathcal{X}^k), \\[2mm]
\Lambda_1^{k+1} = \Lambda_1^k + \beta_1(\mathcal{X}^{k+1} - \mathcal{Y}^{k+1}), \\[1mm]
\Lambda_2^{k+1} = \Lambda_2^k + \beta_2(\mathcal{X}^{k+1} - \mathcal{Y}^{k+1}).
\end{cases}
\tag{6}
$$

For $\mathcal{Y}$-subproblem:

$$
\mathcal{Y}^{k+1} = \arg\min_{\mathcal{Y}} ||\mathcal{Y}||_* + \frac{\beta_1}{2}||\mathcal{X}^k - \mathcal{Y} + \frac{\Lambda_1^k}{\beta_1}||_F^2.
\tag{7}
$$

By doing t-SVD, $\mathcal{X}^k + \frac{\Lambda_1^k}{\beta_1}$ can be decomposed into $\mathcal{U} * \mathcal{S} * \mathcal{V}^*$. Then the subproblem can be solved by the singular value

thresholding [14, 15] as:

$$\mathcal{Y}^{k+1} = \mathcal{U} * \mathcal{C}_{\frac{1}{\beta_1}} * \mathcal{V}^*, \tag{8}$$

where $\mathcal{C}_{\frac{1}{\beta_1}}$ is an f-diagonal tensor whose each frontal slice in the Fourier domain is $\bar{\mathcal{C}}_{\frac{1}{\beta_1}}(i,j,k) = (\bar{\mathcal{S}}_{\frac{1}{\beta_1}}(i,j,k) - \frac{1}{\beta_1})_+$.

For $\mathcal{Z}$-subproblem:

$$\mathcal{Z}^{k+1} = \arg \min_{\mathcal{Z}} \lambda\Phi(\mathcal{Z}) + \frac{\beta_2}{2}||\mathcal{X}^k - \mathcal{Z} + \frac{\Lambda_2^k}{\beta_2}||_F^2, \tag{9}$$

treating $\mathcal{X}^k + \frac{\Lambda_2^k}{\beta_2}$ as the corrupted tensor, this subproblem can be regarded as a denoising problem with the regularizer $\Phi(\mathcal{Z})$. Given a regularizer $\Phi(\mathcal{Z})$, we have a corresponding denoiser to tackle with the denoising problem. Instead of tailoring nonlocal regularizers, we promote the self-similarity by off-the-shell denoiser. The idea is known as regularization by denoising (RED) [16] which is also named plug-and-play (PnP) [13]. Particularly, in the TNN model, we find that the residual image of the recovered image and original image follows the Gaussian distribution (see Fig.1). Inspired by RED, there are many off-the-shelf Gaussian denoiser to solve the subproblem, e.g. BM3D [17], CBM3D [18], VBM3D [19], and ITSReg [20]. For instance, when processing color images, we select CBM3D [18] denoiser to update $\mathcal{Z}$, i.e. ,

$$\mathcal{Z}^{k+1} = \text{CBM3D}(\mathcal{X}^k + \frac{\Lambda_2^k}{\beta_2}, \sigma), \tag{10}$$

where σ (the value of σ see Section 4) is determined by λ and β_2. The parameter σ is linked to the noise level in i.i.d Gaussian denoising, but here the σ is linked to the general system error between $\mathcal{X}^k + \frac{\Lambda_2^k}{\beta_2}$ and the original tensor.

For $\mathcal{X}$-subproblem:

$$\mathcal{X}^{k+1} = \arg\min_{\mathcal{X}} \frac{\beta_1}{2}||\mathcal{X}^k - \mathcal{Y} + \frac{\Lambda_1^k}{\beta_1}||_F^2 \\ + \frac{\beta_2}{2}||\mathcal{X}^k - \mathcal{Z} + \frac{\Lambda_2^k}{\beta_2}||_F^2 + \iota(\mathcal{X}). \tag{11}$$

This is a quadratic optimization problem which has the following closed-form solution:

$$\mathcal{X}^{k+1} = \mathcal{P}_{\Omega^C}(\frac{\beta_1\mathcal{Y}^{k+1} + \beta_2\mathcal{Z}^{k+1} - \Lambda_1^k - \Lambda_2^k}{\beta_1 + \beta_2}) + \mathcal{P}_\Omega(\mathcal{M}).$$

3.3. Convergence

Although the effectiveness of PnP ADMM has been widely proved, its convergence is still an open problem. Fortunately, the convergence of our plug-and-play instance is guaranteed, since the denoiser is a proximity operator [21].

| The original image | The recovered image | The residual image |
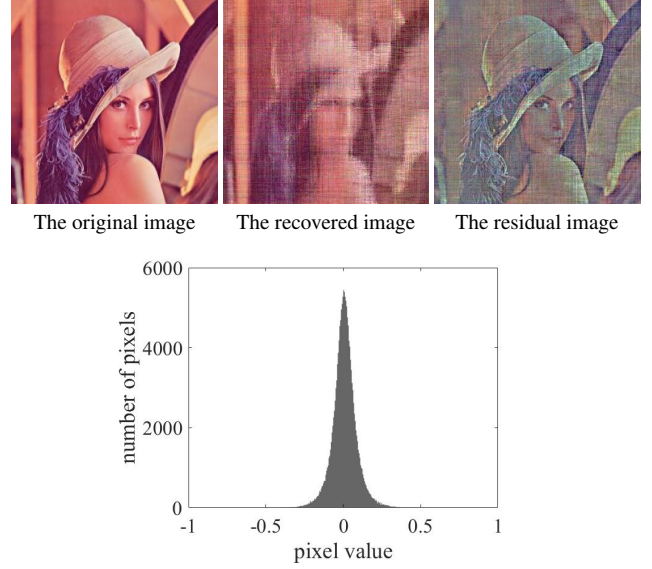
Fig. 1: The first row: the original image, the recovered image by TNN, and the residual image between the original image and the recovered image. The second row: the histogram of the residual image.

4. EXPERIMENTS

We evaluate the performance of the proposed method, named global low-tubal-rankness and nonlocal self-similarity (LTR-NSS) on two kinds of tensor: color images and fluorescence microscope images. The peak signal to noise rate (PSNR) and the structural similarity index (SSIM) [22] are selected as the performance evaluation indices.

All parameters of proposed methods are fine-tuned to achieve the highest PSNR value. The parameter β_1 and β_2 are self-adapting which times ρ each iteration. The parameter λ are typically selected from the set $\{10^{-1}, 10^{-2}, 10^{-3}\}$, and the initial value of parameters β_1 and β_2 are selected from the set $\{10^{-1}, 10^{-2}, 10^{-3}, 10^{-4}\}$. The compared methods include TNN [9], HaLRTC [23], and TNN-3DTV [24]. And the parameters of compared methods are selected to reach their best performance referring to the related papers [9, 23, 24]. We normalized all images to the range of $[0, 1]$. Each image is the size of $256 \times 256 \times 3$.
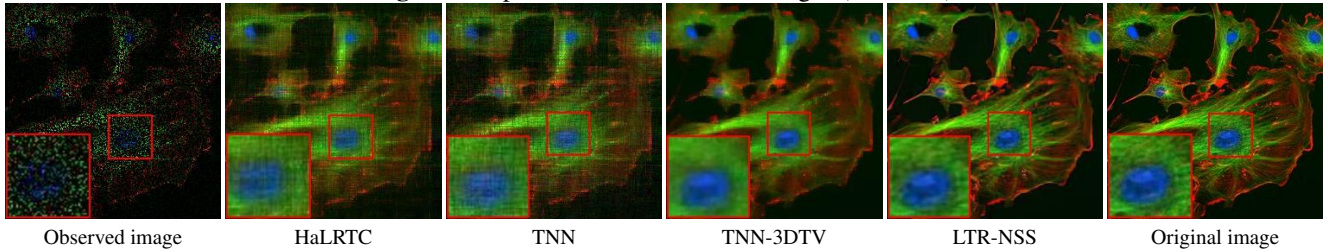
4.1. Color Image Completion

In this experiment, we selected two color images named *lena* and *barbara*. The observed tensors are randomly sampled by pixel and the sampling rates (SR) are 10%, 20%, and 30%, respectively. We selected CBM3D as the denoiser because this Gaussian denoiser works by nonlocal self-similarity and performs excellently in color image denoising. We set $\lambda = 0.01$, $\beta_1 = \beta_2 = 0.1$, $\rho = 1.1$, and $\sigma = 1/\lambda\beta_2^{\frac{1}{\sqrt{k}}}$. The σ gets smaller as the iteration goes on because the general system error is getting smaller.

Table 1: PSNR and SSIM values of the results by different methods. The **best** and <u>second</u> values are highlighted in bold and underline, respectively.

Images		PSNR				SSIM			
		HaLRTC	TNN	TNN-3DTV	LTR-NSS	HaLRTC	TNN	TNN-3DTV	LTR-NSS
Lena	10%	19.36	18.95	<u>22.97</u>	**28.52**	0.4425	0.3483	<u>0.7123</u>	**0.8866**
$256 \times 256 \times 3$	20%	22.74	22.78	<u>26.11</u>	**32.09**	0.6176	0.5543	<u>0.8202</u>	**0.9378**
	30%	25.33	25.49	<u>28.08</u>	**34.42**	0.7433	0.6969	<u>0.8766</u>	**0.9612**
Barbara	10%	18.39	18.24	<u>21.92</u>	**28.66**	0.4056	0.3591	<u>0.6496</u>	**0.9006**
$256 \times 256 \times 3$	20%	21.86	21.89	<u>25.05</u>	**33.29**	0.6044	0.5682	<u>0.7840</u>	**0.9571**
	30%	24.30	24.72	<u>26.93</u>	**36.02**	0.7335	0.7161	<u>0.8466</u>	**0.9754**

| Observed image | HaLRTC | TNN | TNN-3DTV | LTR-NSS | Original image |

Fig. 2: Completion results for color images (SR=20%).

| Observed image | HaLRTC | TNN | TNN-3DTV | LTR-NSS | Original image |

Fig. 3: Completion results for fluorescence microscope images (SR=20%).

Tab. 1 shows the PSNR and SSIM values of different methods. It shows that the proposed method outperforms other methods both on PSNR and SSIM. The TNN and HaLRTC achieve similar result and TNN-3DTV achieves the second high PSNR and SSIM values with the power of TV regularizer which expresses piecewise smoothing prior.

Completion results of different methods are illustrated partly in Fig. 2 (SR=20%). Visually, it can be seen that our proposed method performs best and the details are nicely recovered.

4.2. Fluorescence Microscope Image Completion

In this subsection, fluorescence microscope images were selected to test our proposed model. As fluorescence sample images are mostly images of observed cells, the images have the property of nonlocal self-similarity. CBM3D is still adopted to process such images. We set $\beta_1 = \beta_2 = 0.1$, $\lambda = 0.1$, $\rho = 1.1$, and $\sigma = 1/\lambda\beta_2^{\frac{1}{\sqrt{k}}}$. The completion results of different methods are illustrated in Fig.3. It can be seen that our method gains superior performance to compared methods.

5. CONCLUSION

In this work, we designed a novel tensor completion model, which takes both the global correlation and nonlocal self-similarity into consideration. The TNN guarantees the low-rankness of tensor and the denoiser selected appropriately focuses on nonlocal self-similarity in real-data. An efficient PnP ADMM framework was developed to tackle the proposed model with guaranteed convergence. Numerical experiments on different tensor data showed the superiority of our method over many state-of-the-art methods.

REFERENCES

[1] C. J. Hillar and L.-H. Lim, "Most tensor problems are np-hard," *Journal of the ACM*, vol. 60, no. 6, p. 45, 2013.

[2] W.-H. Xu, X.-L. Zhao, T.-Y. Ji, J.-Q. Miao, T.-H. Ma, S. Wang, and T.-Z. Huang, "Laplace function based nonconvex surrogate for low-rank tensor completion," *Signal Processing: Image Communication*, vol. 73, pp. 62–69, 2019.

[3] J.-H. Yang, X.-L. Zhao, T.-H. Ma, Y. Chen, T.-Z. Huang, and M. Ding, "Remote sensing images destriping using unidirectional hybrid total variation and nonconvex low-rank regularization," *Journal of Computational and Applied Mathematics*, vol. 363, pp. 124–144, 2020.

[4] Y.-B. Zheng, T.-Z. Huang, T.-Y. Ji, X.-L. Zhao, T.-X. Jiang, and T.-H. Ma, "Low-rank tensor completion via a smooth matrix factorization," *Applied Mathematical Modelling*, vol. 70, pp. 677–695, 2019.

[5] M. E. Kilmer and C. D. Martin, "Factorization strategies for third-order tensors," *Linear Algebra and its Applications*, vol. 435, no. 3, pp. 641–658, 2011.

[6] K. Braman, "Third-order tensors as linear operators on a space of matrices," *Linear Algebra and its Applications*, vol. 433, no. 7, pp. 1241–1253, 2010.

[7] C. D. Martin, R. Shafer, and B. LaRue, "An order-p tensor factorization with applications in imaging," *SIAM Journal on Scientific Computing*, vol. 35, no. 1, pp. A474–A490, 2013.

[8] M. E. Kilmer, K. Braman, N. Hao, and R. C. Hoover, "Third-order tensors as operators on matrices: A theoretical and computational framework with applications in imaging," *SIAM Journal on Matrix Analysis and Applications*, vol. 34, no. 1, pp. 148–172, 2013.

[9] Z. Zhang, G. Ely, S. Aeron, N. Hao, and M. Kilmer, "Novel methods for multilinear data completion and de-noising based on tensor-svd," in *Proceedings of the IEEE conference on Computer Vision and Pattern Recognition*, 2014, pp. 3842–3849.

[10] C. Lu, J. Feng, Y. Chen, W. Liu, Z. Lin, and S. Yan, "Tensor robust principal component analysis: Exact recovery of corrupted low-rank tensors via convex optimization," in *Proceedings of the IEEE Conference on Computer Vision and Pattern Recognition*, 2016, pp. 5249–5257.

[11] O. Semerci, N. Hao, M. E. Kilmer, and E. L. Miller, "Tensor-based formulation and nuclear norm regularization for multienergy computed tomography," *IEEE Transactions on Image Processing*, vol. 23, no. 4, pp. 1678–1693, 2014.

[12] Q. Xie, Q. Zhao, D. Meng, and Z. Xu, "Kronecker-basis-representation based tensor sparsity and its applications to tensor recovery," *IEEE Transactions on Pattern Analysis and Machine Intelligence*, vol. 40, no. 8, pp. 1888–1902, 2018.

[13] S. H. Chan, X. Wang, and O. A. Elgendy, "Plug-and-play admm for image restoration: Fixed-point convergence and applications," *IEEE Transactions on Computational Imaging*, vol. 3, no. 1, pp. 84–98, 2016.

[14] J.-F. Cai, E. J. Candès, and Z. Shen, "A singular value thresholding algorithm for matrix completion," *SIAM Journal on Optimization*, vol. 20, no. 4, pp. 1956–1982, 2010.

[15] A. S. Lewis, "The convex analysis of unitarily invariant matrix functions," *Journal of Convex Analysis*, vol. 2, no. 1, pp. 173–183, 1995.

[16] Y. Romano, M. Elad, and P. Milanfar, "The little engine that could: Regularization by denoising (RED)," *SIAM Journal on Imaging Sciences*, vol. 10, no. 4, pp. 1804–1844, 2017.

[17] K. Dabov, A. Foi, V. Katkovnik, and K. Egiazarian, "Image denoising by sparse 3-D transform-domain collaborative filtering," *IEEE Transactions on Image Processing*, vol. 16, no. 8, pp. 2080–2095, 2007.

[18] K. Dabov, A. Foi, V. Katkovnik, and K. O. Egiazarian, "Color image denoising via sparse 3D collaborative filtering with grouping constraint in luminance-chrominance space." in *IEEE International Conference on Image Processing*, 2007, pp. 313–316.

[19] K. Dabov, A. Foi, and K. Egiazarian, "Video denoising by sparse 3d transform-domain collaborative filtering," in *15th European Signal Processing Conference*. IEEE, 2007, pp. 145–149.

[20] Q. Xie, Q. Zhao, D. Meng, Z. Xu, S. Gu, W. Zuo, and L. Zhang, "Multispectral images denoising by intrinsic tensor sparsity regularization," in *Proceedings of the IEEE Conference on Computer Vision and Pattern Recognition*, 2016, pp. 1692–1700.

[21] C. Paris, J. Bioucas-Dias, and L. Bruzzone, "A novel sharpening approach for superresolving multiresolution optical images," *IEEE Transactions on Geoscience and Remote Sensing*, vol. 57, no. 3, pp. 1545–1560, 2018.

[22] Z. Wang, A. C. Bovik, H. R. Sheikh, E. P. Simoncelli *et al.*, "Image quality assessment: from error visibility to structural similarity," *IEEE Transactions on Image Processing*, vol. 13, no. 4, pp. 600–612, 2004.

[23] J. Liu, P. Musialski, P. Wonka, and J. Ye, "Tensor completion for estimating missing values in visual data," *IEEE Transactions on Pattern Analysis and Machine Intelligence*, vol. 35, no. 1, pp. 208–220, 2012.

[24] F. Jiang, X.-Y. Liu, H. Lu, and R. Shen, "Anisotropic total variation regularized low-rank tensor completion based on tensor nuclear norm for color image inpainting," in *2018 IEEE International Conference on Acoustics, Speech and Signal Processing*. IEEE, 2018, pp. 1363–1367.